





Article

In Vitro Activity Assays of Sputtered HAp Coatings with SiC Addition in Various Simulated Biological Fluids

Alina Vlădescu ^{1,2} , Anca Pârâu ¹, Iulian Pană ¹ , Cosmin M. Cotruț ^{2,3} , Lidia R. Constantin ¹, Viorel Braic ¹ and Diana M. Vranceanu ^{3,*} 

¹ Department for Advanced Surface Processing and Analysis by Vacuum Technologies, National Institute of Research and Development for Optoelectronics—INOE 2000, 409 Atomistilor St., RO77125 Magurele, Romania; alinava@inoe.ro (A.V.); anca.parau@inoe.ro (A.P.); iulian.pana@inoe.ro (I.P.); lidia.constantin@inoe.ro (L.R.C.); vbraic@inoe.ro (V.B.)

² Physical Materials Science and Composite Materials Centre, National Research Tomsk Polytechnic University, Lenin Avenue 43, Tomsk 634050, Russia; cosmin.cotrut@upb.ro

³ Department of Metallic Materials Science, Physical Metallurgy, University Politehnica of Bucharest, 313 Spl. Independentei, RO60042 Bucharest, Romania

* Correspondence: diana.vranceanu@upb.ro; Tel.: +40-21-366-953

Received: 13 May 2019; Accepted: 13 June 2019; Published: 15 June 2019



Abstract: Considering the requirements of medical implantable devices, it is pointed out that biomaterials should play a more sophisticated, longer-term role in the customization and optimization of the material–tissue interface in order to ensure the best long-term clinical outcomes. The aim of this contribution was to assess the performance of silicon carbide–hydroxyapatite in various simulated biological fluids (Dulbecco’s modified Eagle’s medium (DMEM), simulated body fluid (SBF), and phosphate buffer solution (PBS)) through immersion assays for 21 days at 37 ± 0.5 °C and to evaluate the electrochemical behavior. The coatings were prepared on Ti6Al4V alloy substrates by magnetron sputtering method using two cathodes made of hydroxyapatite and silicon carbide (SiC). After immersion assays the coating’s surface was analyzed in terms of morphology, chemical and phase composition, and chemical bonds. According to the electrochemical behavior in the media investigated at 37 ± 0.5 °C, SiC addition inhibits the dissolution of the hydroxyapatite in DMEM acellular media. Furthermore, after adding SiC, the slow degradation of hydroxyapatite in PBS and SBF media as well as biomineralization in DMEM were observed.

Keywords: SBF; DMEM; PBS; hydroxyapatite; silicon; magnetron sputtering

1. Introduction

Nowadays, great efforts are dedicated to the development of biomaterials with tunable properties. One of the proposed solutions is the usage of calcium phosphate (CaP)-based coatings. Today’s trends in medicine and bioengineering indicate that by using active biomaterials, a more prompt, enhanced, and improved healing process will take place without eliciting any adverse immune rejection reactions [1–4]. Due to its remarkable properties and similarity with the inorganic phase of the bone, hydroxyapatite (HAp), the most known “member” of the CaP family, has been extensively used as both a bulk bioactive ceramic and/or a coating in medical applications [5–9].

Considering the requirements of medical implantable devices, it is pointed out that the biomaterials should play a more sophisticated, longer-term role in the customization and optimization of the material–tissue interface in order to ensure the best long-term clinical outcomes [1–4,10].

The biofunctionality and in vitro abilities of HAp can be adjusted by controlling its phase, structure, composition, and morphology. One way to achieve this is by incorporating/adding different elements such as F [11], Mg [12–17], Zn [12,17–21], Ag [16,19,22], Sr [13,17,23], and Si [24–29] into the HAp structure, which is very flexible. A considerable number of scientific papers related to the substitution of HAp with various elements can be found in the literature, indicating that this is an important path in the biomaterial and medical fields. The doping/addition elements have been selected either due to their properties or because they can be found in natural human bone in quantities ranging from wt.% to ppm levels [30,31]. Regardless of the selection criteria, they exhibit a beneficial influence on the overall abilities, characteristics, and properties of HAp.

In order to predict the biomaterials' in vivo behavior, initial tests should be performed in vitro by monitoring the formation of an apatite layer and/or the degradation of the biomaterial [32]. When talking about HAp degradation, the dissolution rate in the human body environment is considered a key indicator, because HAp needs to be biologically resorbed by the body within a certain period after implantation, leading to an enhanced osseointegration. Consequently, from the bioactivity point of view, the substitution of hydroxyapatite with different elements could be the most suitable solution for decreasing the dissolution rate of hydroxyapatite, giving enough time for the strong anchorage of the implant [25].

In our previous papers [33–35], we aimed and succeeded to enhance the mechanical properties of sputtered hydroxyapatite coatings by adding SiC into their structure without affecting their osseointegration and bioactive characteristics. According to our studies, SiC addition improved the hardness and elastic modulus of HAp coating, this being a positive effect for materials used in biomedical applications. Also, we showed that SiC-added HAp coating has a superior electrochemical behavior in artificial saliva, being a good solution for dental applications. Moreover, we showed that Ag addition into HAp coating increases its antibacterial abilities without affecting its bioactivity or biomineralization abilities [22].

According to Mertz [36], silicon can be considered a key element, being indispensable for health, while Carlisle [37] suggested that silicon not only has a structural role but also a metabolic role in hard connective tissues. Moreover, it has been indicated that silicon is involved in bone formation through the synthesis and/or stabilization of collagen. Its presence was found at the mineralization front of growing bone [38], suggesting an involvement in early the calcification/mineralization of the bone matrix. Thus, silicon was selected for addition into the HAp structure, because it is an essential trace element found in small quantities in bones and other major organs, and its lack has been associated with bone and joint diseases [39–43].

In the present study, we immersed Hap + SiC samples in different biological media such as Dulbecco's modified Eagle's medium (DMEM), simulated body fluid (SBF), and phosphate buffer solution (PBS) for 21 days at 37 ± 0.5 °C to analyze their effect and to observe if these coatings are also a good choice for orthopedic applications. Because we want to highlight the use of the proposed coatings as potential candidates for orthopedic applications as well, we selected the three media mentioned above due to their similarity to the human environment and because they are frequently mentioned in biocompatibility assays and electrochemical behavior. Moreover, by using three media that present few similarities and major differences concerning their chemical compositions, a wider vision can be obtained concerning the biomaterial's behavior. Regardless of the available data, there is limited information on the behavior of HAp + SiC coatings obtained by the magnetron sputtering method inacellular media (DMEM, SBF, and PBS).

To highlight the electrochemical behavior of the coatings, electrochemical measurements at 37 ± 0.5 °C in all three media were performed. To the best of our knowledge, such study is not present in the literature and it is our belief that this investigation will provide valuable information to the scientific community. The influence of SiC addition has been previously investigated in terms of physicochemical, mechanical, and in vitro biocompatibility assays (cell viability/cytotoxicity assays) and a positive influence on the HAp structure and cell behavior was noted [33,34]. The present study

intends to expand the research on HAp + SiC coatings and add some valuable results by performing in vitro assays in different acellular media (DMEM, SBF, and PBS).

2. Materials and Methods

The coatings were prepared using an RF-magnetron sputtering method onto both Ti6Al4V alloy and Si wafer substrates. For the deposition, two cathodes with a 1 inch diameter of hydroxyapatite and SiC (99.9% purity, Kurt J. Lesker Co., Hastings, UK) were used. The Si wafer was used as a substrate only for the phase compositions of HAp and the HAp with the addition of SiC. The following deposition conditions were carried out: base pressure = 1.3×10^{-4} Pa; Ar pressure = 6.6×10^{-1} Pa; RF power fed on both hydroxyapatite cathodes = 50 W; RF power fed on SiC cathode = 15 W; bias voltage = −60 V; deposition temperature = 700 °C. These parameters were carefully chosen based on our earlier results published in [33–35].

SiC-added hydroxyapatite coatings were tested in vitro in order to study their behavior in the following simulated biological fluids: (1) DMEM prepared from DMEM powder (Sigma Aldrich, Darmstadt, Germany); (2) SBF prepared according to Kokubo's recipe [44]; and (3) PBS prepared by using PBS tablets (Sigma Aldrich, Darmstadt, Germany). The pH for all three media was adjusted to 7.4 by dropwise addition of 1 M HCl and 1 M NaOH for SBF and sodium bicarbonate for DMEM. All three media used for these assays yield valuable information about the coating behavior in the simulated biological system and their chemical compositions are presented in Table 1. The immersion assays were performed according to ISO/FDIS 23317:2007 [45].

Table 1. Chemical composition of acellular media simulated body fluid (SBF), Dulbecco's modified Eagle's medium (DMEM), and phosphate buffer solution (PBS) in comparison with human blood plasma.

Chemical Composition		Human Blood Plasma	Acellular Media		
			SBF	DMEM [46,47]	PBS
Ion Concentration (mM)	Na ⁺	142	142	154.5	137
	K ⁺	5	5	5.4	2.7
	Mg ²⁺	1.5	1.5	0.8	–
	Ca ²⁺	2.5	2.5	1.8	–
	Cl [−]	103	148.8	120.5	–
	HCO ₃ [−]	27	4.2	44	–
	HPO ₄ [−]	1	1	0.9	10
	SO ₄ ^{2−}	0.5	–	0.8	–
Buffer			TRIS and 1 M HCl	No	NaHCO ₃
pH		7.2–7.4	7.4	7.4	7.4
Amino Acids		N/A	No	0.084 g/L L-Arginine · HCl	No
				0.042 g/L L-Histidine · HCl · H ₂ O	
				0.105 g/L L-Isoleucine	
				0.105 g/L L-Leucine	
				0.146 g/L L-Lysine · HCl	
				0.03 g/L L-Methionine	
				0.066 g/L L-Phenylalanine	
				0.042 g/L L-Serine	
				0.095 g/L L-Threonine	
				0.016 g/L L-Tryptophan	
				0.10379 g/L L-Tyrosine, 2Na · 2H ₂ O	
				0.094 g/L L-Valine	

Table 1. Cont.

Chemical Composition	Human Blood Plasma	Acellular Media		
		SBF	DMEM [46,47]	PBS
Vitamins	N/A	No	0.004 g/L Choline Chloride 0.004 g/L Folic Acid 0.0072 g/L Myo-Inositol 0.004 g/L Niacinamide 0.004 g/L D-Pantothenic Acid · $\frac{1}{2}$ Ca 0.004 g/L Pyridoxal · HC 0.0004 g/L Riboflavin 0.004 g/L Thiamine · HCl	No
Other Components	N/A	No	1.0 g/L D-Glucose 0.0159 g/L Phenol Red · Na 0.11 g/L Pyruvic Acid · Na	No

After the in vitro immersion experiments, the following analyses were carried out (Figure 1):

- Elemental composition and morphology using a scanning electron microscope (SEM, Hitachi TM3030Plus, Tokyo, Japan) equipped with energy dispersive spectrometry (EDS, Bruker);
- Mass evolution, which was monitored gravimetrically using an analytical balance (ALT 100-5AM, Kern, Balingen, Germany) with an accuracy of 0.01 mg;
- Phase composition by grazing-incidence XRD (X-ray diffraction) using Cu K α radiation (SmartLab, Rigaku, Tokyo, Japan) from 10° to 80° with a step size of 0.02°/min and an incident angle of 2°;
- Chemical binding by Fourier transform infrared spectroscopy at a resolution of 4 cm⁻¹, over the frequency range of 500–4000 cm⁻¹ using an FTIR-6300 spectrophotometer (Jasco, Tokyo, Japan) with a universal Pike MIRacle attenuated total reflectance (ATR) sampling accessory (Pike Technologies, Madison, WI, USA).

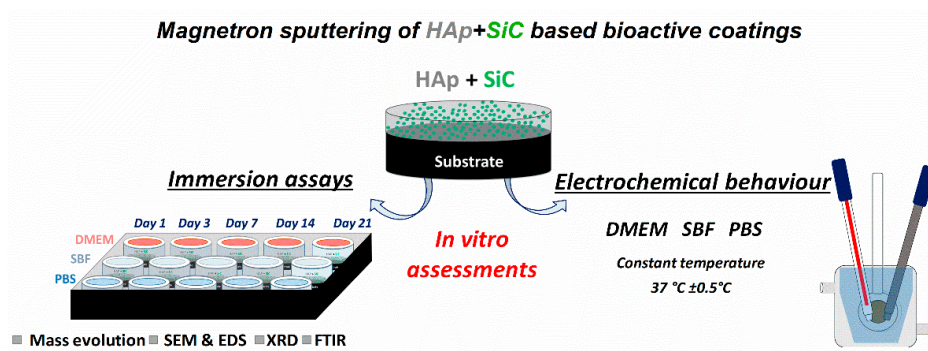


Figure 1. Schematic illustration of the experimental setup and analysis.

The in vitro electrochemical behavior was achieved using a PARSTAT 4000 Potentiostat/Galvanostat (Princeton Applied Research, Princeton, NJ, USA) coupled with a Low Current Interface (VersaSTAT LC, Princeton Applied Research) to evaluate the behavior of HAp + SiC coatings in all three simulated biological media (DMEM, SBF, and PBS). The tests were carried out in a typical three-electrode electrochemical cell applying the following protocol:

- An area of 1 cm² was exposed to the acellular media, placing the sample in the working electrode (WE—a Teflon sample holder);
- A platinum electrode was used as the counter electrode (CE);
- A saturated calomel (SCE) as the reference electrode (RE).

All measurements were achieved according to the ASTM G5–94 standard (reapproved 2011) at a scanning rate of 1 mV/s. The open circuit potential (OCP) was monitored for 1 h, starting right after the

sample's immersion in the electrolyte, and the potentiodynamic curves were recorded from ± 250 mV vs. the open circuit potential (E_{oc}).

For initial assessment of the potential bioactivity of a material, the apatite formation occurring in vivo was reproduced in vitro in different acellular media [44,48–53].

3. Results and Discussions

3.1. SEM and EDS after Immersion in DMEM, SBF, and PBS

It is well documented that both biomineralization and biodegradation processes/phenomena occur either simultaneously and/or in competition with each other due to chemical reactivity [54–56]. Thus, based on all of these, a bioactive surface will slightly dissolve in time, favoring the formation of a new apatite layer and promoting the formation of chemical bonds directly on the hard tissue [57–60]. Meanwhile, through biodegradation, regardless of the mechanism that leads to the material removal/resorption, the tissue will grow directly in all the irregularities found on the surface without it being necessary for the interface to interact directly with the material [25,54,61–67].

SEM images of each sample after its exposure in DMEM, SBF, and PBS can be observed in Figure 2. In order to show details of the mechanism of biomineralization/degradation, the EDS results are also presented in Figure 2.

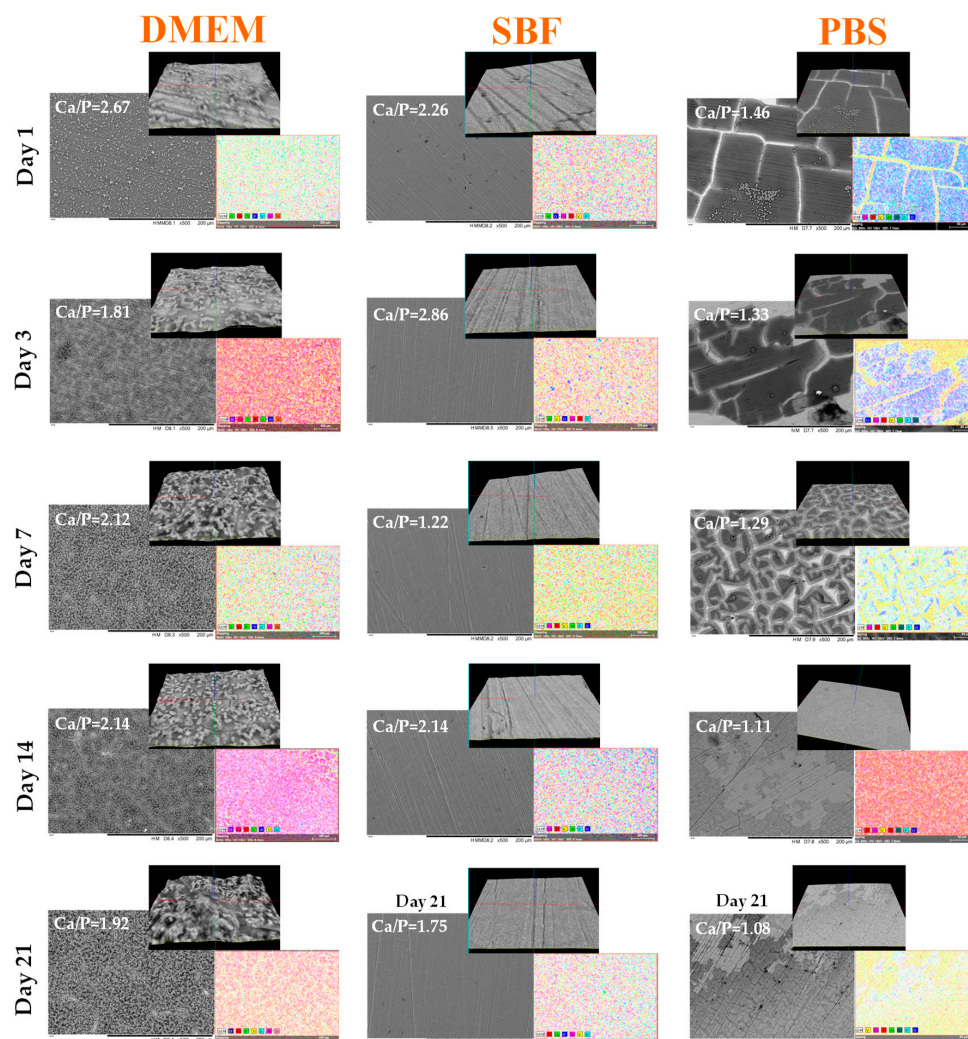


Figure 2. 2D, 3D SEM images and energy dispersive spectrometry (EDS) mapping of the coated surfaces after immersion in all three acellular media.

Note that the coatings before biomineralization tests exhibited a Ca/P ratio of about 1.67 ± 0.02 . The SEM images of surfaces before biomineralization are published in [34]. Thorough characterization of the HAp and SiC-doped HAp coatings in terms of phase composition, topography and surface texture, adhesion between the coating and substrate, chemical bonds, and mechanical properties (hardness and elastic modulus) can be found in previous publications [33–35]. Due to the dissolution/precipitation mechanism that occurs at the interface between HAp + SiC and the testing media, the Ca/P ratio of the HAp + SiC coating after immersion presented modifications which sustained the degradation and/or led to biomineralization.

According to the SEM images, the coated surfaces immersed in PBS suffered a degradation process that was initiated at the beginning of the tested 21 days. It is necessary to specify that in the literature the apatite formation mechanism starts with the partial dissolution of calcium ions from HAp, which then react with phosphate ions in PBS to form apatite [68,69].

This result is also confirmed by the EDS analysis, which showed that the Ca/P ratio decreased by increasing the immersion time. From this it can be assumed that the dissolution process is predominant and not balanced by the apatite precipitation. It is worth mentioning that PBS is a balanced salt solution commonly used in biological research due to its resemblance to human extracellular fluid, and it has also been used in degradation studies [70–73].

In SBF media, the developed layer also presented signs indicating partial degradation. For SBF acellular media, the EDS results indicated a Ca/P ratio above 2, suggesting the formation of a layer consisting of Ca-enriched hydroxyapatite. The SEM and EDS results of the coatings immersed in DMEM clearly showed the formation of new apatite phases, which increased with increasing the immersion time. Moreover, the chemical composition of the media influenced the HAp + SiC behavior. This was more visible for DMEM which, besides its similar ion concentrations with SBF, contains amino acids, vitamins, and other components that favor the precipitation of new apatite phases. However, further studies need to be performed in order to provide a wider perspective.

In the light of the aforementioned observations, it can be assumed that the HAp + SiC coatings presented some areas that are susceptible to the dissolution process, leading to their degradation, while other areas remained stable, as it can be seen in Figure 2.

In PBS, the coatings started their degradation from the first day of immersion, initially presenting signs of cracks followed by areas of delamination from the substrate surface. Starting on day 14, larger areas without coating could be observed, indicating that the coating was more or less dissolved by the media. Overall it can be said that the coatings were more affected by the PBS and SBF solutions than by DMEM.

3.2. Mass Evolution in DMEM, SBF, and PBS

The mass evolution of the coatings immersed in DMEM, SBF, and PBS over 1, 3, 7, 14, and 21 days is presented in Figure 3. It is generally known that the newly formed apatite layer is accepted as a hallmark of the bioactive materials and it is assumed to enable the quick formation of a mechanically stable and functional interface at the biomaterial–tissue level.

For the coatings immersed in SBF and PBS, the lost mass increased with increasing the immersion time, signifying that the coatings were degraded in these two media. Regarding the coatings immersed in DMEM, the mass increased with the immersion time, demonstrating good mineralization abilities. This effect was more obvious after 21 days of immersion. With respect to the acellular media used in this study, it can be said that DMEM presents not only different types of salts but also vitamins, proteins, and other nutrients, while SBF and PBS acellular media present some similarities in terms of their chemical compositions. Nevertheless, Porter et al. [74] hypothesized that the different behavior of HAp + SiC could also be associated with the number and types of structural defects present in the coatings. They suggested that a higher number of defects could lead to an increased solubility and, consequently, a more elevated bone apposition rate, following a process of dissolution/precipitation [31].

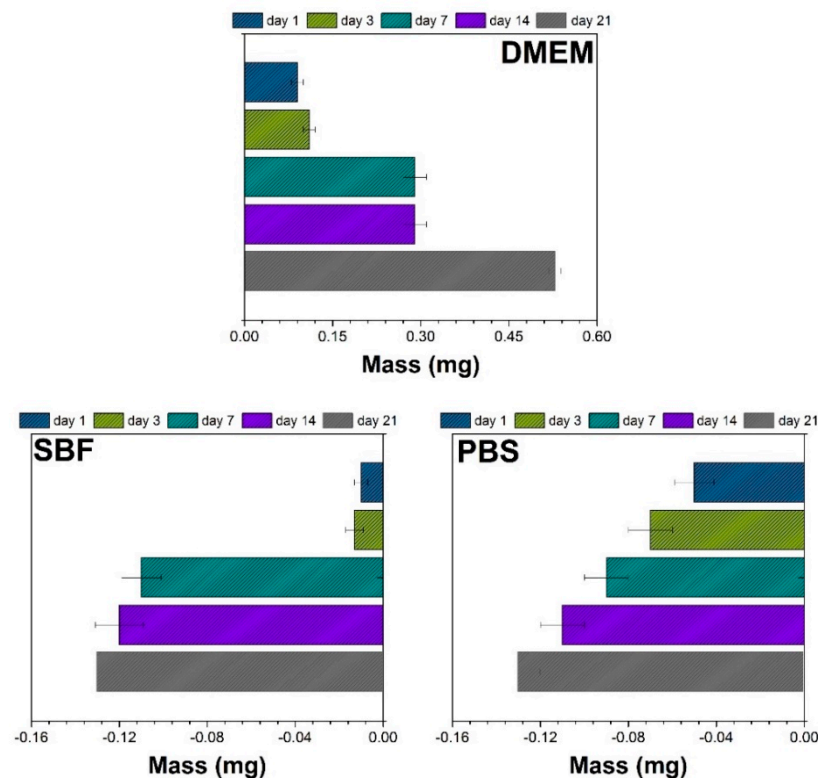


Figure 3. Apatite mass evolution of the coatings exposed to DMEM, SBF, and PBS.

All things considered, it is possible that due to the preparation method, the developed coatings may have presented some compactness defects, thus influencing the films' behavior in the acellular media. All together, these results suggest that in the presence of proteins, a higher interaction at the HAp + SiC and acellular media level is observed, thus limiting the coating degradation. According to a study by Schwarz, Si can bind to connective tissue and its components, specifically glycosaminoglycans, polysaccharides, and mucopolysaccharides [75], although the mechanism by which this occurs is yet to be elucidated. Moreover, Hench et al. [76] suggested that such materials have been shown to present higher bonding abilities to bone compared to their counterparts without Si by the spontaneous formation of a biologically active apatite-like layer on their surface.

3.3. XRD after Immersion in DMEM, SBF, and PBS

Figure 4 presents the XRD diffractograms of HAp + SiC compared to HAp before their immersion in the testing media. As can be seen, the characteristic peaks according to ICDD#09-0432 standard are present in the HAp structure and no other secondary phase was detected. It can be observed that the HAp XRD pattern is distorted. This finding is probably due to the Si peak from the substrate (Si-ICDD#04-002-0118 standard). In the XRD pattern of undoped HAp, there is a peak located around 10.8° with high intensity which can also be attributed to the brushite phase. It is well known that the acquisition of an XRD diffractogram often favors preferential crystal orientations, especially the phases with highly anisotropic morphologies such as brushite. In most cases, experimental XRD peaks may be significantly different compared to calculated ones, by variation in peak intensities. Drouet demonstrated that the (020) experimental peak becomes more intense than expected for randomly oriented crystals for brushite [77]. He also reported that these modifications will separate brushite from the apatite compounds. Based on this published conclusion, we believe that it is possible that other CaP phases such as brushite may form around 10.8° . To sustain this state, a more complex analysis should be conducted, which is a further aim of our research.

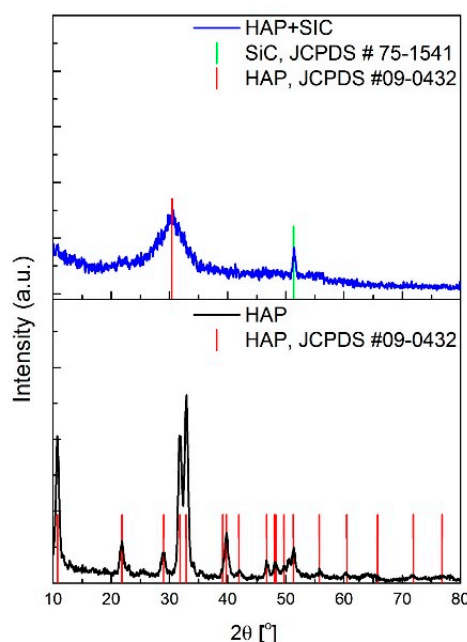


Figure 4. X-ray diffraction (XRD) patterns of the coatings before immersion in acellular media (the substrate is an Si wafer; Si identification is based on the ICDD#04-002-0118 standard).

With the addition of SiC, the XRD diffractogram changed its pattern and not all HAp peaks were detected, a fact which suggests that the coating tends towards amorphization due to the increase of nucleation, which leads to the reduction of grain size. Overall, SiC addition reduced the crystallinity of HAp and one peak characteristic for SiC and HAp was detected by XRD analysis. Moreover, it is clear that with SiC addition, the HAp peak observed in the HAp + SiC coatings shifted towards lower angles. This indicates that some structural changes, such as HAp elemental cell deformation, occurred. These findings are in good correlation with the findings of other researchers [78,79].

XRD diffraction patterns of the coated surfaces after immersion in DMEM, SBF, and PBS are presented in Figure 5. For the samples tested in DMEM, a broad line at the beginning can be observed, which could be a sign of an amorphous phase formation. Moreover, the line located at 63.6° , attributed to hydroxyapatite, is diminished with increasing the immersion time, suggesting a controlled release.

For samples immersed in SBF, the lines of hydroxyapatite overlap those of the bare substrate, making it difficult to state the presence or absence of apatite phases. After 3 days of immersion, some peaks found at 10.7° , 21.5° , 31.7° , 45.3° , and 56.6° are visible, and were attributed to the HAp phase. These peaks present diminished intensities after 7 days of immersion, indicating the degradation of the coating (supported by the mass loss presented in Figure 3), which thus favors the growth of new bone tissue.

No discussion about other peaks was performed because all of these can be attributed to both the substrate and hydroxyapatite. Regardless of the immersion time, the XRD lines of the coatings immersed in PBS are all similar, indicating that in this case the XRD is not an adequate method for recoding the changes undergone by the coatings after immersion.

Thus, the surfaces were analyzed by the FTIR technique, which is more sensitive than XRD for confirming the new apatite phases formed after immersion in all media.

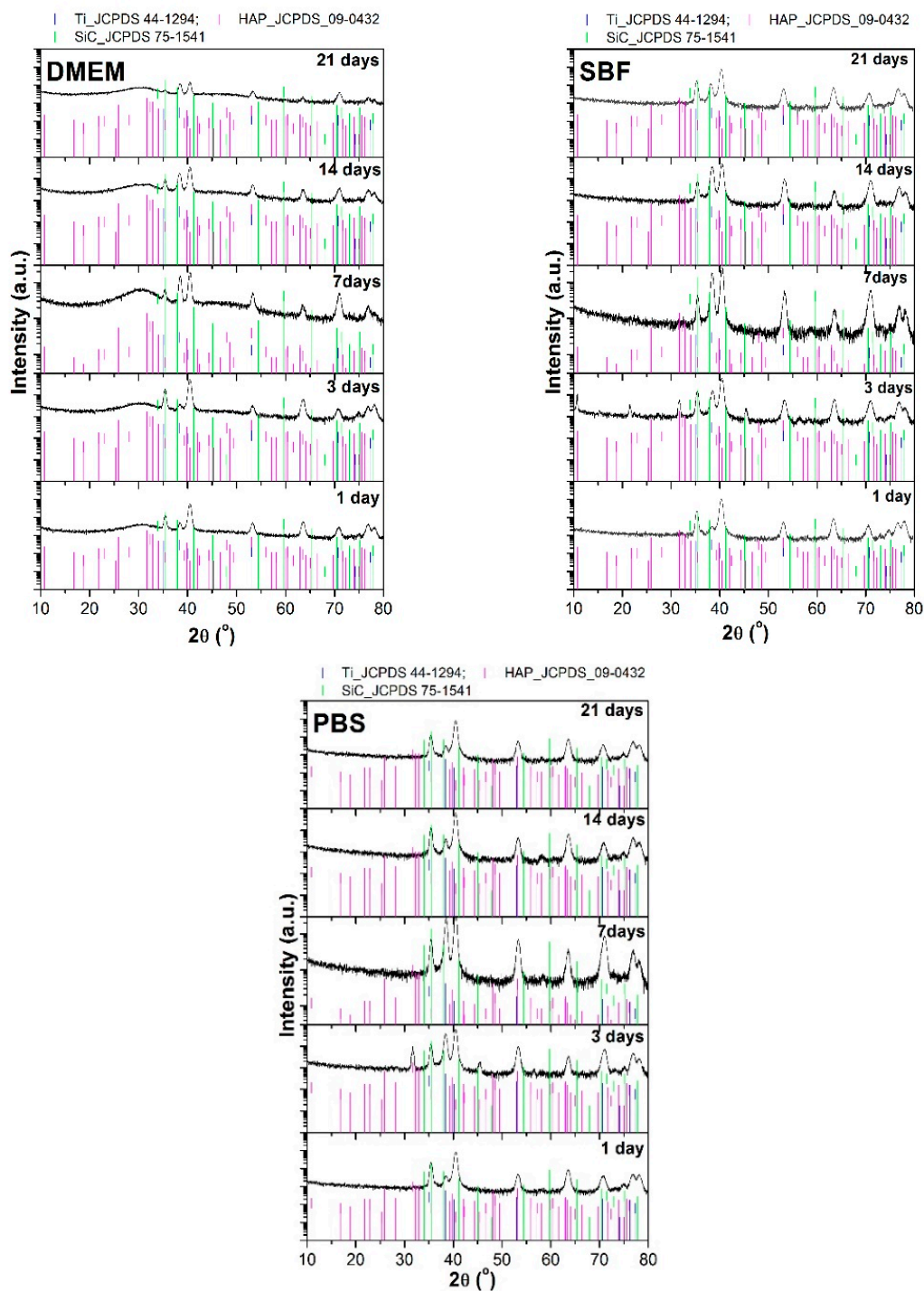


Figure 5. XRD diffraction patterns of coated surfaces after immersion in DMEM, SBF, and PBS (Ti6Al4V alloy is the substrate).

3.4. FTIR after Immersion in DMEM, SBF, and PBS

Figure 6 presents the FTIR spectra for HAp and HAp + SiC coatings before immersion in DMEM, SBF, or PBS. The typical bands for HAp were observed—1087, 1034, and 962 cm^{-1} —assigned to the presence of the P–O functional group. As it can be observed, the IR bands became wider and shifted towards lower wavenumbers after the addition of SiC into the HAp structure. Moreover, no specific absorption bands located between 770 and 680 cm^{-1} [34,80], corresponding to SiC stretching bonds, were revealed by FTIR analysis. Thus, it can be assumed that the addition of SiC led to

some modifications in the HAp structure; some additional bands at 928 and 906 cm^{-1} were observed. According to the literature, these bands can be attributed to PO_4^{4-} or SiO_4^{4-} vibrational modes, because both chemical groups share similarly spaced vibrational modes due to the similarities of PO_4^{4-} and SiO_4^{4-} tetrahedral molecular units [81].

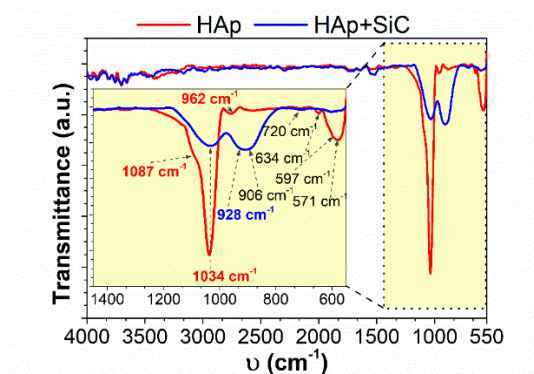


Figure 6. FTIR spectra of HAp and HAp + SiC before immersion in acellular media.

The band intensity corresponding to 962 cm^{-1} in HAp was less evident for the HAp + SiC coating. This finding can be explained by the broad band located around 930 cm^{-1} , which also includes the line from 962 cm^{-1} .

FTIR spectra of the coated surfaces after immersion in DMEM, SBF, or PBS are presented in Figure 7. The FTIR spectra provided lines similar to each other, which can be attributed to hydroxyapatite. Hydroxyl stretch, with its typical bands located between 3500 and 3200 cm^{-1} [82,83], can be observed just for the coatings immersed in SBF. These peaks are visible for the surfaces immersed for 3 and 14 days with a lower intensity and are completely invisible for the samples immersed for 1, 7, and 21 days. For the samples immersed in SBF for 3 and 7 days, a much diminished peak attributed to hydroxyl can be observed, indicating that some phosphates groups were still present on the surface.

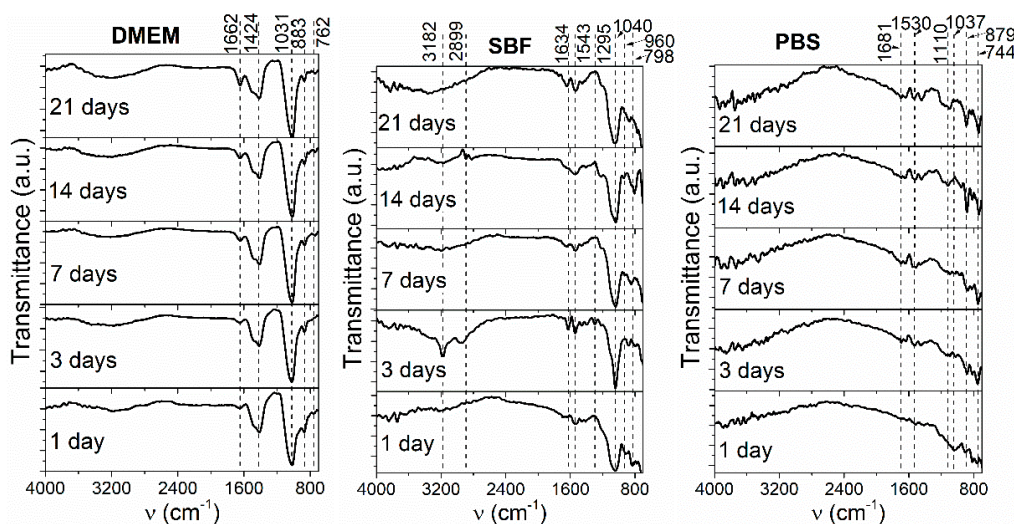


Figure 7. FTIR spectra of the coated surfaces after immersion in DMEM, SBF, and PBS.

No hydroxyl bands were seen for the coatings immersed in DMEM or PBS, regardless of the immersion time. This finding is probably due to the addition of Si into the HAp structure, which led to a reduction of hydroxyl peaks due to the extra negative charge of the silicate group, compensated by the loss of OH^- . Nakata et al. suggested that this charge is a consequence of the bonding change and

symmetry of the phosphate groups which takes place due to Si addition [84]. Carbonate bands can be usually found around 873 cm^{-1} (ν_2) and in the region of 1650 to 1300 cm^{-1} (ν_3) [83,85–87].

The samples immersed in all solutions exhibit more or less visible carbonate bands. For the coatings immersed in SBF or PBS, these bands have a lower intensity, while for DMEM they are more intense. This finding is probably due to the competition between the phosphate and carbonate ions.

Phosphate has bands at 1190 – 976 (ν_3) cm^{-1} , 961 (ν_1) cm^{-1} , 469 (ν_2) cm^{-1} , and 660 – 520 (ν_4) cm^{-1} [83,86,88]. Considering our results, two weak peaks at 798 and 960 cm^{-1} can be found and one stronger peak at 1040 cm^{-1} for the coatings immersed in SBF. The intensity of the band found at 1040 cm^{-1} increases with the immersion time, indicating the formation of a new phosphate phase. For the coatings immersed in DMEM, a strong peak at 1031 cm^{-1} is observed, which is almost similar for each immersion time. For the coatings tested in PBS, the bands of phosphate appear after 3 days of immersion and grow higher after 14 days, indicating the formation of new phases. This result could be indicative of the good mineralization abilities of the coated surfaces. The FTIR spectra for the coatings immersed in PBS are noisier due to the roughness of the newly formed CaP phases.

The FTIR spectra indicate that there are some differences between the samples immersed in the investigated solutions. The most obvious change is the significant decrease of the hydroxyl peak. The hydroxyl peaks are absent in the case of the coatings immersed in DMEM and PBS. The intensity of peaks observed in the spectra of samples immersed in PBS is lower, indicating that the phase found on this surface has a low crystallinity degree.

On the other hand, the presence of the CO_3^{2-} group indicates an apatite-based structure slightly deficient in Ca [86,89]. For the samples tested in PBS and DMEM, a peak located at 880 cm^{-1} is evident, which according to the literature can be assigned to the formation of a non-stoichiometric hydroxyapatite structure [86,89]. Moreover, this peak can be also attributed to the carbonate phase. The bands ranging from 1400 to 1500 cm^{-1} , as well as those at 880 cm^{-1} , demonstrate the substitution of phosphate groups with carbonate groups in the hydroxyapatite matrix [89–92].

3.5. In Vitro Electrochemical Performance of SiC–HA_p Coatings in DMEM, SBF, and PBS

Tafel plots of the investigated coatings in DMEM, SBF, and PBS solutions are presented in Figure 8. From the Tafel plots, the electrochemical parameters were calculated and are presented in Table 2. It can be seen that the coatings had a better electrochemical behavior in DMEM, as compared with PBS and SBF. The coatings exhibited an almost similar evolution in PBS and SBF media.

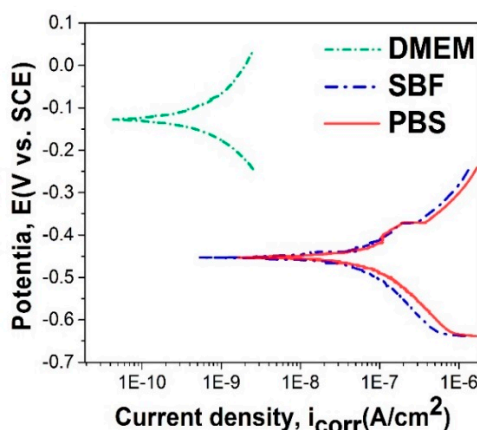


Figure 8. Tafel plots of the coated samples in DMEM, SBF, and PBS acellular media at $37 \pm 0.5\text{ }^{\circ}\text{C}$.

Taking into consideration the values presented in Table 2, it can be concluded that:

- Coated samples tested in DMEM have a more electropositive value of corrosion potential (E_{corr}), indicating a better electrochemical behavior, while in PBS and SBF the values are similar;

- The lowest value of the corrosion current density (i_{corr}) was recorded for coated samples tested in DMEM, followed by those in SBF and then those in PBS;
- The polarization resistance (R_p) is higher for coated samples tested in DMEM, followed by those in PBS and those in SBF.

Table 2. Electrochemical parameters calculated based on Tafel extrapolation.

Electrolyte	E_{corr} (mV)	i_{corr} (nA/cm ²)	R_p (k Ω ·cm ²)
DMEM	−126	1.90	54,652.6
SBF	−453	89.73	474.4
PBS	−454	108.02	364.9

The electrochemical tests showed that the Ti6Al4V coated with SiC–HAp had a better behavior in DMEM but was affected by SBF and PBS, being less resistant in PBS. After electrochemical experiments the surface morphology and chemical composition were investigated by SEM and EDS, and the obtained images and elements distribution are presented in Figure 9.

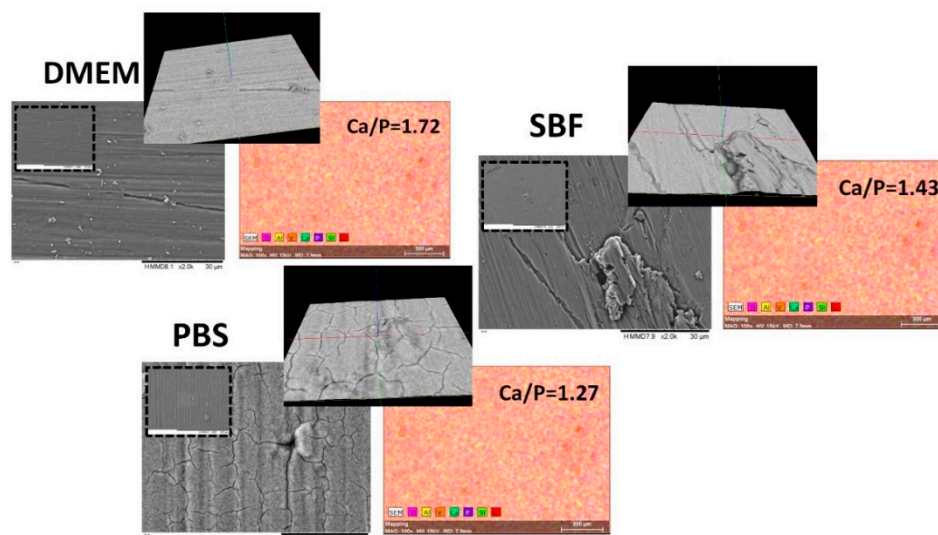


Figure 9. SEM images, element distribution, and Ca/P ratio of the HAp + SiC coatings after in vitro electrochemical measurements in DMEM, SBF, and PBS.

As it can be seen, the coatings were visibly degraded in PBS when compared to DMEM and SBF. Nevertheless, the sample in PBS media registered the lowest Ca/P ratio with a value of 1.27 when compared to that in SBF media (ratio of 1.43) and DMEM (ratio of 1.72). SEM images also revealed that PBS favors the appearance and propagation of cracks in the HAp + SiC coating, a phenomenon that was not visible for the coatings immersed in SBF and DMEM.

4. Conclusions

Coatings prepared by the addition of SiC into hydroxyapatite by magnetron sputtering were prepared for the present study. This study showed that the addition of SiC into HAp provides new aspects of biological processes involved in the osseointegration capabilities of these bioceramic-based coatings.

The performed in vitro assays led to the following conclusions:

- The in vitro electrochemical measurements highlighted that the Ti6Al4V coated with HAp + SiC films had a better electrochemical behavior in DMEM as compared with PBS and SBF, which present a higher Cl^- content as compared with DMEM;

- The immersion assays performed for 21 days showed that in SBF and PBS media, the HAp + SiC films presented signs of degradation and the reported data were comparable (mass loss of ~0.13 mg on day 21), while in DMEM the coatings demonstrated good mineralization abilities (a gained mass of ~0.53 mg on day 21);
- The XRD patterns achieved on the HAp + SiC coatings after their immersion pointed out the appearance of peaks characteristic to a newly formed apatite-based phase, but which either disappear or overlap the substrate over the immersion period;
- FTIR analysis performed on the HAp + SiC coatings showed differences in the spectra shape with respect to the immersion testing media, and characteristic phosphate bands were registered in all three media.

All three media used for these assays yield valuable information about the future behavior of the proposed implantable biomaterial in biological systems and, based on the results presented in this paper, which correlated with the results obtained in previous papers, the proposed coatings were found to be potential materials suitable for use in medical applications.

Author Contributions: C.M.C. and A.V. designed the research and supervised the work; D.M.V., A.P., I.P., and L.R.C. performed the experiments; V.B. prepared the coatings. A.V. and C.M.C. analyzed the data and provided valuable input in data interpretation; D.M.V. and A.V. wrote the first draft of the article; all authors reviewed and approved the work.

Funding: The work was supported by the grant of the Romanian National Authority for Scientific Research and Innovation, CCCDI-UEFISCDI, Project no. 117PED/2017 (DegraCoat), within PNCDI III, as well the Core Program of 2019 (no. 18N/2019). The EDS, SEM, and XRD results were acquired using the systems purchased by the Sectorial Operational Programme “Increase of Economic Competitiveness”, ID 1799/SMIS 48589/2015. Also the PROINSTITUTIO Project no. 19PFE/17.10.2018 was used for financial support.

Conflicts of Interest: The authors declare no conflict of interest.

References

1. Poitout, D.G. *Biomechanics and Biomaterials in Orthopedics*; Springer: London, UK, 2016; ISBN 978-1-84882-663-2.
2. Sugawara, E.; Nikaido, H. Properties of AdeABC and AdeIJK efflux systems of *Acinetobacter baumannii* compared with those of the AcrAB-TolC system of *Escherichia coli*. *Antimicrob. Agents Chemother.* **2014**, *58*, 7250–7257. [[CrossRef](#)] [[PubMed](#)]
3. Ivanova, E.P.; Bazaka, K.; Crawford, R.J. *New Functional Biomaterials for Medicine and Healthcare*; Woodhead Publishing: Cambridge, UK, 2014; ISBN 9781782422655.
4. Bhat, S.; Kumar, A. Biomaterials and bioengineering tomorrow’s healthcare. *Biomatter* **2013**, *3*, e24717. [[CrossRef](#)] [[PubMed](#)]
5. Rau, J.-V.; Cacciotti, I.; Laureti, S.; Fosca, M.; Varvaro, G.; Latini, A. Bioactive, nanostructured Si-substituted hydroxyapatite coatings on titanium prepared by pulsed laser deposition. *J. Biomed. Mater. Res. Part B Appl. Biomater.* **2015**, *103*, 1621–1631. [[CrossRef](#)] [[PubMed](#)]
6. Dorozhkin, S.V. Calcium orthophosphates: Occurrence, properties, biomineralization, pathological calcification and biomimetic applications. *Biomatter* **2011**, *1*, 121–164. [[CrossRef](#)] [[PubMed](#)]
7. Mocanu, A.-C.; Stan, G.E.; Maidaniuc, A.; Miculescu, M.; Antoniac, I.V.; Ciocoiu, R.-C.; Voicu, Ş.I.; Mitran, V.; Cîmpean, A.; Miculescu, F. Naturally-derived biphasic calcium phosphates through increased phosphorus-based reagent amounts for biomedical applications. *Materials* **2019**, *12*, 381. [[CrossRef](#)]
8. Gómez-Morales, J.; Iafisco, M.; Delgado-López, J.M.; Sarda, S.; Drouet, C. Progress on the preparation of nanocrystalline apatites and surface characterization: Overview of fundamental and applied aspects. *Prog. Cryst. Growth Charact. Mater.* **2013**, *59*, 1–46. [[CrossRef](#)]
9. Dorozhkin, S.V. Calcium orthophosphates (CaPO₄): Occurrence and properties. *Morphologie* **2017**, *101*, 125–142. [[CrossRef](#)]
10. Kasemo, B.; Lausmaa, J. Material-tissue interfaces: The role of surface properties and processes. *Environ. Health Perspect.* **1994**, *102*, 41–45. [[CrossRef](#)]
11. Karamian, E.; Abdellahi, M.; Khandan, A.; Abdellah, S. Introducing the fluorine doped natural hydroxyapatite-titania nanobiocomposite ceramic. *J. Alloy. Compd.* **2016**, *679*, 375–383. [[CrossRef](#)]

12. Dasgupta, S.; Banerjee, S.S.; Bandyopadhyay, A.; Bose, S. Zn- and Mg-doped hydroxyapatite nanoparticles for controlled release of protein. *Langmuir* **2010**, *26*, 4958–4964. [[CrossRef](#)]
13. Roy, M.; Bandyopadhyay, A.; Bose, S. Induction plasma sprayed Sr and Mg doped nano hydroxyapatite coatings on Ti for bone implant. *J. Biomed. Mater. Res. Part B Appl. Biomater.* **2011**, *99*, 258–265. [[CrossRef](#)] [[PubMed](#)]
14. Mishra, V.K.; Bhattacharjee, B.N.; Parkash, O.; Kumar, D.; Rai, S.B. Mg-doped hydroxyapatite nanoplates for biomedical applications: A surfactant assisted microwave synthesis and spectroscopic investigations. *J. Alloy. Compd.* **2014**, *614*, 283–288. [[CrossRef](#)]
15. Mansour, S.F.; El-dek, S.I.; Dorozhkin, S.V.; Ahmed, M.K. Physico-mechanical properties of Mg and Ag doped hydroxyapatite/chitosan biocomposites. *New J. Chem.* **2017**, *41*, 13773–13783. [[CrossRef](#)]
16. Gozalian, A.; Behnamghader, A.; Daliri, M.; Moshkforoush, A. Synthesis and thermal behavior of Mg-doped calcium phosphate nanopowders via the sol gel method. *Sci. Iran.* **2011**, *18*, 1614–1622. [[CrossRef](#)]
17. Kaygili, O.; Keser, S. Sol-gel synthesis and characterization of Sr/Mg, Mg/Zn and Sr/Zn co-doped hydroxyapatites. *Mater. Lett.* **2015**, *141*, 161–164. [[CrossRef](#)]
18. Robles-Águila, M.J.; Reyes-Avendaño, J.A.; Mendoza, M.E. Structural analysis of metal-doped (Mn, Fe, Co, Ni, Cu, Zn) calcium hydroxyapatite synthesized by a sol-gel microwave-assisted method. *Ceram. Int.* **2017**, *43*, 12705–12709. [[CrossRef](#)]
19. Samani, S.; Hossainipour, S.M.; Tamizifar, M.; Rezaie, H.R. In vitro antibacterial evaluation of sol-gel-derived Zn-, Ag-, and (Zn + Ag)-doped hydroxyapatite coatings against methicillin-resistant *Staphylococcus aureus*. *J. Biomed. Mater. Res. Part A* **2013**, *101*, 222–230. [[CrossRef](#)]
20. Yuan, Q.; Wu, J.; Qin, C.; Xu, A.; Zhang, Z.; Lin, Y.; Chen, Z.; Lin, S.; Yuan, Z.; Ren, X.; et al. One-pot synthesis and characterization of Zn-doped hydroxyapatite nanocomposites. *Mater. Chem. Phys.* **2017**, *199*, 122–130. [[CrossRef](#)]
21. Prosolov, K.A.; Belyavskaya, O.A.; Rau, J.V.; Prymak, O.; Epple, M.; Sharkeev, Y.P. Deposition of polycrystalline zinc substituted hydroxyapatite coatings with a columnar structure by RF magnetron sputtering: Role of in-situ substrate heating. *J. Phys. Conf. Ser.* **2018**, *1115*, 032077. [[CrossRef](#)]
22. Vranceanu, D.M.; Parau, A.C.; Cotrut, C.M.; Kiss, A.E.; Constantin, L.R.; Braic, V.; Vladescu, A. In vitro evaluation of Ag doped hydroxyapatite coatings in acellular media. *Ceram. Int.* **2019**, *45*, 11050–11061. [[CrossRef](#)]
23. Huang, Y.; Ding, Q.; Pang, X.; Han, S.; Yan, Y. Corrosion behavior and biocompatibility of strontium and fluorine co-doped electrodeposited hydroxyapatite coatings. *Appl. Surf. Sci.* **2013**, *282*, 456–462. [[CrossRef](#)]
24. Manzano, M.; Lozano, D.; Arcos, D.; Portal-Núñez, S.; la Orden, C.L.; Esbrit, P.; Vallet-Regí, M. Comparison of the osteoblastic activity conferred on Si-doped hydroxyapatite scaffolds by different osteostatin coatings. *Acta Biomater.* **2011**, *7*, 3555–3562. [[CrossRef](#)] [[PubMed](#)]
25. Vallet-Regí, M.; Arcos, D. Silicon substituted hydroxyapatites. A method to upgrade calcium phosphate based implants. *J. Mater. Chem.* **2005**, *15*, 1509–1516. [[CrossRef](#)]
26. Qiu, Z.-Y.; Noh, I.-S.; Zhang, S.-M. Silicate-doped hydroxyapatite and its promotive effect on bone mineralization. *Front. Mater. Sci.* **2013**, *7*, 40–50. [[CrossRef](#)]
27. Martínez-Vázquez, F.J.; Cabañas, M.V.; Paris, J.L.; Lozano, D.; Vallet-Regí, M. Fabrication of novel Si-doped hydroxyapatite/gelatin scaffolds by rapid prototyping for drug delivery and bone regeneration. *Acta Biomater.* **2015**, *15*, 200–209. [[CrossRef](#)] [[PubMed](#)]
28. Astala, R.; Calderín, L.; Yin, X.; Stott, M.J. Ab initio simulation of Si-doped hydroxyapatite. *Chem. Mater.* **2006**, *18*, 413–422. [[CrossRef](#)]
29. Zhao, X.; Yang, J.; Xin, H.; Wang, X.; Zhang, L.; He, F.; Liu, Q.; Zhang, W. Improved dispersion of SiC whisker in nano hydroxyapatite and effect of atmospheres on sintering of the SiC whisker reinforced nano hydroxyapatite composites. *Mater. Sci. Eng. C* **2018**, *91*, 135–145. [[CrossRef](#)] [[PubMed](#)]
30. Blumenthal, N.C.; Betts, F.; Posner, A.S. Effect of carbonate and biological macromolecules on formation and properties of hydroxyapatite. *Calcif. Tissue Res.* **1975**, *18*, 81–90. [[CrossRef](#)] [[PubMed](#)]
31. Patel, N.; Best, S.M.; Bonfield, W.; Gibson, I.R.; Hing, K.A.; Damien, E.; Revell, P.A. A comparative study on the in vivo behavior of hydroxyapatite and silicon substituted hydroxyapatite granules. *J. Mater. Sci. Mater. Med.* **2002**, *13*, 1199–1206. [[CrossRef](#)] [[PubMed](#)]
32. Kokubo, T.; Yamaguchi, S. Novel bioactive materials developed by simulated body fluid evaluation: Surface-modified Ti metal and its alloys. *Acta Biomater.* **2016**, *44*, 16–30. [[CrossRef](#)] [[PubMed](#)]

33. Vranceanu, D.M.; Cotrut, C.M.; Bramowicz, M.; Titorencu, I.; Kulesza, S.; Kiss, A.; Berbecaru, A.; Pruna, V.; Branzei, M.; Vladescu, A. Osseointegration of sputtered SiC-added hydroxyapatite for orthopaedic applications. *Ceram. Int.* **2016**, *42*, 10085–10093. [[CrossRef](#)]
34. Vladescu, A.; Birlik, I.; Braic, V.; Toparli, M.; Celik, E.; Ak Azem, F. Enhancement of the mechanical properties of hydroxyapatite by SiC addition. *J. Mech. Behav. Biomed. Mater.* **2014**, *40*, 362–368. [[CrossRef](#)] [[PubMed](#)]
35. Azem, F.A.; Kiss, A.; Birlik, I.; Braic, V.; Luculescu, C.; Vladescu, A. The corrosion and bioactivity behavior of SiC doped hydroxyapatite for dental applications. *Ceram. Int.* **2014**, *40*, 15881–15887. [[CrossRef](#)]
36. Mertz, W. Human requirements: Basic and optimal. *Ann. N. Y. Acad. Sci.* **1972**, *199*, 191–201. [[CrossRef](#)]
37. Carlisle, E.M. Silicon as a trace nutrient. *Sci. Total Environ.* **1988**, *73*, 95–106. [[CrossRef](#)]
38. Carlisle, E.M. Silicon as an essential trace element in animal nutrition. In *Silicon Biochemistry Ciba Foundation Symposium 121*; Evered, D., O'Connor, M., Eds.; John Wiley & Sons: Chichester, UK, 2007; pp. 123–139.
39. Schwarz, K.; Milne, D.B. Growth-promoting effects of silicon in rats. *Nature* **1972**, *239*, 333–334. [[CrossRef](#)] [[PubMed](#)]
40. Iyengar, G.V. Reference values for the concentrations of As, Cd, Co, Cr, Cu, Fe, I, Hg, Mn, Mo, Ni, Pb, Se, and Zn in selected human tissues and body fluids. *Biol. Trace Elem. Res.* **1987**, *12*, 263–295. [[CrossRef](#)] [[PubMed](#)]
41. Jugdaohsingh, R.; Pedro, L.D.; Watson, A.; Powell, J.J. Silicon and boron differ in their localization and loading in bone. *Bone Rep.* **2015**, *1*, 9–15. [[CrossRef](#)]
42. Zhuoer, H.; Environmental, G.; Republic, P. Silicon measurement in bone and other tissues by electrothermal atomic absorption spectrometry. *J. Anal. At. Spectrom.* **1994**, *9*, 11–15. [[CrossRef](#)]
43. Carlisle, E.M. Silicon: A requirement in bone formation independent of vitamin D1. *Calcif. Tissue Int.* **1981**, *33*, 27–34. [[CrossRef](#)]
44. Kokubo, T.; Takadama, H. How useful is SBF in predicting in vivo bone bioactivity? *Biomaterials* **2006**, *27*, 2907–2915. [[CrossRef](#)] [[PubMed](#)]
45. *ISO/FDIS 23317 Implants for Surgery—In Vitro Evaluation for Apatite-Forming Ability of Implant Materials*; International Organization for Standardization (ISO): Geneva, Switzerland, 2007.
46. Faure, J.; Balamurugan, A.; Benhayoune, H.; Torres, P.; Balossier, G.; Ferreira, J.M.F. Morphological and chemical characterisation of biomimetic bone like apatite formation on alkali treated Ti6Al4V titanium alloy. *Mater. Sci. Eng. C* **2009**, *29*, 1252–1257. [[CrossRef](#)]
47. Rohanová, D.; Boccaccini, A.R.; Horkavcová, D.; Bozděchová, P.; Bezdička, P.; Častorálová, M. Is non-buffered DMEM solution a suitable medium for in vitro bioactivity tests? *J. Mater. Chem. B* **2014**, *2*, 5068–5076. [[CrossRef](#)]
48. Vladescu, A.; Vranceanu, D.M.; Kulesza, S.; Ivanov, A.N.; Bramowicz, M.; Fedonnikov, A.S.; Braic, M.; Norkin, I.A.; Koptug, A.; Kurtukova, M.O.; et al. Influence of the electrolyte's pH on the properties of electrochemically deposited hydroxyapatite coating on additively manufactured Ti64 alloy. *Sci. Rep.* **2017**, *7*, 16819. [[CrossRef](#)]
49. Li, P.; Ohtsuki, C.; Kokubo, T.; Nakanishi, K.; Soga, N.; Nakamura, T.; Yamamuro, T. Effects of ions in aqueous media on hydroxyapatite induction by silica gel and its relevance to bioactivity of bioactive glasses and glass-ceramics. *J. Appl. Biomater.* **1993**, *4*, 221–229. [[CrossRef](#)] [[PubMed](#)]
50. Kokubo, T.; Kushitani, H.; Ohtsuki, C.; Sakka, S.; Yamamuro, T. Effects of ions dissolved from bioactive glass-ceramic on surface apatite formation. *J. Mater. Sci. Mater. Med.* **1993**, *4*, 1–4. [[CrossRef](#)]
51. Wu, C.; Xiao, Y. Evaluation of the in vitro bioactivity of bioceramics. *Bone Tissue Regen. Insights* **2009**, *2009*, 25–29. [[CrossRef](#)]
52. De Aza, P.N.; Guitian, F.; Merlos, A.; Lora-Tamayo, E.; De Aza, S. Bioceramics—Simulated body fluid interfaces: pH and its influence of hydroxyapatite formation. *J. Mater. Sci. Mater. Med.* **1996**, *7*, 399–402. [[CrossRef](#)]
53. Hench, L.L. Bioceramics: From concept to clinic. *J. Am. Ceram. Soc.* **1991**, *74*, 1487–1510. [[CrossRef](#)]
54. Dorozhkin, S.V. Inorganic chemistry of the dissolution phenomenon: The dissolution mechanism of calcium apatites at the atomic (ionic) level. *Comments Inorg. Chem.* **1999**, *20*, 285–299. [[CrossRef](#)]
55. Dorozhkin, S.V. A review on the dissolution models of calcium apatites. *Prog. Cryst. Growth Charact. Mater.* **2002**, *44*, 45–61. [[CrossRef](#)]
56. Dorozhkin, S.V. Calcium orthophosphates (CaPO₄): Occurrence and properties. *Prog. Biomater.* **2016**, *5*, 9–70. [[CrossRef](#)] [[PubMed](#)]

57. LeGeros, R.Z. Calcium phosphate-based osteoinductive materials. *Chem. Rev.* **2008**, *108*, 4742–4753. [[CrossRef](#)] [[PubMed](#)]
58. Šupová, M. Substituted hydroxyapatites for biomedical applications: A review. *Ceram. Int.* **2015**, *41*, 9203–9231. [[CrossRef](#)]
59. Orly, I.; Gregoire, M.; Menanteau, J.; Heughebaert, M.; Kerebel, B. Chemical changes in hydroxyapatite biomaterial under in vivo and in vitro biological conditions. *Calcif. Tissue Int.* **1989**, *45*, 20–26. [[CrossRef](#)] [[PubMed](#)]
60. Sun, L.; Berndt, C.C.; Gross, K.A.; Kucuk, A. Material fundamentals and clinical performance of plasma-sprayed hydroxyapatite coatings: A review. *J. Biomed. Mater. Res.* **2001**, *58*, 570–592. [[CrossRef](#)] [[PubMed](#)]
61. Pietak, A.M.; Reid, J.W.; Stott, M.J.; Sayer, M. Silicon substitution in the calcium phosphate bioceramics. *Biomaterials* **2007**, *28*, 4023–4032. [[CrossRef](#)] [[PubMed](#)]
62. Kim, S.R.; Lee, J.H.; Kim, Y.T.; Riu, D.H.; Jung, S.J.; Lee, Y.J.; Chung, S.C.; Kim, Y.H. Synthesis of Si, Mg substituted hydroxyapatites and their sintering behaviors. *Biomaterials* **2003**, *24*, 1389–1398. [[CrossRef](#)]
63. Barrère, F.; van der Valk, C.M.; Dalmeijer, R.A.J.; van Blitterswijk, C.A.; de Groot, K.; Layrolle, P. In vitro and in vivo degradation of biomimetic octacalcium phosphate and carbonate apatite coatings on titanium implants. *J. Biomed. Mater. Res. Part A* **2003**, *64*, 378–387. [[CrossRef](#)]
64. Raynaud, S.; Champion, E.; Lafon, J.P.; Bernache-Assollant, D. Calcium phosphate apatites with variable Ca/P atomic ratio III. Mechanical properties and degradation in solution of hot pressed ceramics. *Biomaterials* **2002**, *23*, 1081–1089. [[CrossRef](#)]
65. Wenisch, S.; Stahl, J.-P.; Horas, U.; Heiss, C.; Kilian, O.; Trinkaus, K.; Hild, A.; Schnettler, R. In vivo mechanisms of hydroxyapatite ceramic degradation by osteoclasts: Fine structural microscopy. *J. Biomed. Mater. Res.* **2003**, *67*, 713–718. [[CrossRef](#)] [[PubMed](#)]
66. Dorozhkin, S.V. Dissolution mechanism of calcium apatites in acids: A review of literature. *World J. Methodol.* **2012**, *2*, 1–17. [[CrossRef](#)] [[PubMed](#)]
67. Lu, J.; Descamps, M.; Dejou, J.; Koubi, G.; Hardouin, P.; Lemaitre, J.; Proust, J.-P. The biodegradation mechanism of calcium phosphate biomaterials in bone. *J. Biomed. Mater. Res.* **2002**, *63*, 408–412. [[CrossRef](#)] [[PubMed](#)]
68. Yao, X.; Yao, H.; Li, G.; Li, Y. Biomimetic synthesis of needle-like nano-hydroxyapatite templated by double-hydrophilic block copolymer. *J. Mater. Sci.* **2010**, *45*, 1930–1936. [[CrossRef](#)]
69. Wongwitwichot, P.; Kaewsrirach, J.; Chua, K.H.; Ruzsyzmah, B.H.I. Comparison of TCP and TCP/HA hybrid scaffolds for osteoconductive activity. *Open Biomed. Eng. J.* **2010**, *4*, 279–285. [[CrossRef](#)] [[PubMed](#)]
70. Johnson, I.; Liu, H. A study on factors affecting the degradation of magnesium and a magnesium-yttrium alloy for biomedical applications. *PLoS ONE* **2013**, *8*, e65603. [[CrossRef](#)] [[PubMed](#)]
71. Díaz, E.; Sandonis, I.; Valle, M.B. In vitro degradation of poly(caprolactone)/nHA composites. *J. Nanomater.* **2014**, *2014*, 802435. [[CrossRef](#)]
72. Sumathi, S.; Gopal, B. In vitro degradation of multisubstituted hydroxyapatite and fluorapatite in the physiological condition. *J. Cryst. Growth* **2015**, *422*, 36–43. [[CrossRef](#)]
73. Sheikh, Z.; Zhang, Y.L.; Grover, L.; Merle, G.E.; Tamimi, F.; Barralet, J. In vitro degradation and in vivo resorption of dicalcium phosphate cement based grafts. *Acta Biomater.* **2015**, *26*, 338–346. [[CrossRef](#)]
74. Porter, A.E.; Best, S.M.; Bonfield, W. Ultrastructural comparison of hydroxyapatite and silicon-substituted hydroxyapatite for biomedical applications. *J. Biomed. Mater. Res. Part A* **2004**, *68*, 133–141. [[CrossRef](#)] [[PubMed](#)]
75. Schwarz, K. A bound form of silicon in glycosaminoglycans and polyuronides. *Proc. Natl. Acad. Sci. USA* **1973**, *70*, 1608–1612. [[CrossRef](#)] [[PubMed](#)]
76. Hench, L.L.; Xynos, I.D.; Polak, J.M. Bioactive glasses for in situ tissue regeneration. *J. Biomater. Sci. Polym. Ed.* **2004**, *15*, 543–562. [[CrossRef](#)] [[PubMed](#)]
77. Drouet, C. Apatite formation: Why it may not work as planned, and how to conclusively identify apatite compounds. *Biomed. Res. Int.* **2013**, *2013*, 490946. [[CrossRef](#)] [[PubMed](#)]
78. Balas, F.; Pérez-Pariente, J.; Vallet-Regí, M. In vitro bioactivity of silicon-substituted hydroxyapatites. *J. Biomed. Mater. Res. Part A* **2003**, *66*, 364–375. [[CrossRef](#)] [[PubMed](#)]
79. Yilmaz, B.; Alshemary, A.Z.; Evis, Z. Co-doped hydroxyapatites as potential materials for biomedical applications. *Microchem. J.* **2019**, *144*, 443–453. [[CrossRef](#)]

80. Ouadfel, M.A.; Keffous, A.; Brighet, A.; Gabouze, N.; Hadjersi, T.; Cheriet, A.; Kechouane, M.; Boukezzata, A.; Boukennous, Y.; Belkacem, Y.; et al. Si-rich α - $\text{Si}_{1-x}\text{C}_x$ thin films by d.c. magnetron co-sputtering of silicon and silicon carbide: Structural and optical properties. *Appl. Surf. Sci.* **2013**, *265*, 94–100. [\[CrossRef\]](#)
81. Bianco, A.; Cacciotti, I.; Lombardi, M.; Montanaro, L. Si-substituted hydroxyapatite nanopowders: Synthesis, thermal stability and sinterability. *Mater. Res. Bull.* **2009**, *44*, 345–354. [\[CrossRef\]](#)
82. Czikó, M.; Bogya, E.-S.; Barabás, R.; Bizo, L.; Stefan, R. In vitro biological activity comparison of some hydroxyapatite-based composite materials using simulated body fluid. *Open Chem.* **2013**, *11*, 400372. [\[CrossRef\]](#)
83. Rehman, I.; Bonfield, W. Characterization of hydroxyapatite and carbonated apatite by photo acoustic FTIR spectroscopy. *J. Mater. Sci. Mater. Med.* **1997**, *8*, 1–4. [\[CrossRef\]](#)
84. Nakata, K.; Kubo, T.; Numako, C.; Onoki, T.; Nakahira, A. Synthesis and characterization of silicon-doped hydroxyapatite. *Mater. Trans.* **2009**, *50*, 1046–1049. [\[CrossRef\]](#)
85. Narayan, R.; Bose, S.; Bandyopadhyay, A. *Biomaterials Science: Processing, Properties, and Applications V*; John Wiley & Sons, Inc.: Hoboken, NJ, USA, 2015; ISBN 9781119190134.
86. Berzina-Cimdina, L.; Borodajenko, N. Research of calcium phosphates using fourier transform infrared spectroscopy. In *Infrared Spectroscopy—Materials Science, Engineering and Technology*; IntechOpen: London, UK, 2012; pp. 123–148.
87. Durdu, S.; Deniz, Ö.F.; Kutbay, I.; Usta, M. Characterization and formation of hydroxyapatite on Ti6Al4V coated by plasma electrolytic oxidation. *J. Alloy. Compd.* **2013**, *551*, 422–429. [\[CrossRef\]](#)
88. Mohan, L.; Durgalakshmi, D.; Geetha, M.; Narayanan, T.S.N.S.; Asokamani, R. Electrophoretic deposition of nanocomposite (HAp + TiO_2) on titanium alloy for biomedical applications. *Ceram. Int.* **2012**, *38*, 3435–3443. [\[CrossRef\]](#)
89. Ślósarczyk, A.; Paszkiewicz, Z.; Zima, A. The effect of phosphate source on the sintering of carbonate substituted hydroxyapatite. *Ceram. Int.* **2010**, *36*, 577–582. [\[CrossRef\]](#)
90. Barinov, S.M.; Rau, J.V.; Cesaro, S.N.; Đurišin, J.; Fadeeva, I.V.; Ferro, D.; Medvecky, L.; Trionfetti, G. Carbonate release from carbonated hydroxyapatite in the wide temperature range. *J. Mater. Sci. Mater. Med.* **2006**, *17*, 597–604. [\[CrossRef\]](#) [\[PubMed\]](#)
91. Dorozhkin, S.V. Calcium orthophosphate-based biocomposites and hybrid biomaterials. *J. Mater. Sci.* **2009**, *44*, 2343–2387. [\[CrossRef\]](#)
92. Krishna, D.S.R.; Siddharthan, A.; Seshadri, S.K.; Kumar, T.S.S. A novel route for synthesis of nanocrystalline hydroxyapatite from eggshell waste. *J. Mater. Sci. Mater. Med.* **2007**, *18*, 1735–1743. [\[CrossRef\]](#) [\[PubMed\]](#)

